Inorg. Chem. **2006**, *45*, 8239–8250

Synthesis, Crystal Structure, and Magnetic Studies of One-Dimensional Cyano-Bridged Ln^{3+}–Cr^{3+} Complexes with bpy as a Blocking Ligand

Marta Estrader,[†] Joan Ribas,[†] Vassilis Tangoulis,[#] Xavier Solans,[‡] Merce Font-Bardía,[‡] Miguel Maestro,[§] and Carmen Diaz*,[†]

Departament de Química Inorgànica, Universitat de Barcelona, Martí i Franquès, 1−11, 08028 Barcelona, Spain, Department of Materials Science, University of Patras, 26500 Patras, Greece, Department of Chemistry, Departament de Cristal·lografia Mineralogia i Dipòsits Minerals, Universitat de Barcelona, Martí I Franquès s/n, 08028 Barcelona, Spain, and Departamento de Química Fundamental, Facultade de Ciencias, Universidade da Coruña,15071 A Coruña, Spain

Received May 30, 2006

The reaction of $Ln(NO_3)_3$·aq with $K_3[Cr(CN)_6]$ and 2,2′-bipyridine (bpy) in a water/ethanol solution led to two families of complexes: 4 one-dimensional (1D) complexes of the formula *trans*-$[Cr(CN)_4(\mu\text{-}CN)_2Ln(H_2O)_3(bpy)_2]_n$·$4nH_2O$·$3.5n$bpy ($Ln^{3+}$ = La, Ce, Pr, and Nd) and 10 1D complexes of the formula *trans*-$[Cr(CN)_4(\mu\text{-}CN)_2Ln(H_2O)_4(bpy)]_n$·$3.5nH_2O$·$1.5n$bpy ($Ln^{3+}$ = Nd, Sm, Eu, Tb, Dy, Ho, Er, Tm, Yb, and Lu). The structures for the fourteen complexes $[LaCr]_n$ (**1**), $[CeCr]_n$ (**2**), $[PrCr]_n$ (**3**), $[NdCr]_n$ (**4**), $[NdCr]_n$ (**4′**), $[SmCr]_n$ (**5**), $[EuCr]_n$ (**6**), $[TbCr]_n$ (**7**), $[DyCr]_n$ (**8**), $[HoCr]_n$ (**9**), $[ErCr]_n$ (**10**), $[TmCr]_n$ (**11**), $[YbCr]_n$ (**12**), and $[LuCr]_n$ (**13**) have been solved. Complexes **1**–**4** crystallize in the orthorhombic space group *Pbam* and are isomorphous; complexes **4′**–**13** crystallize in the triclinic space group $P\bar{1}$ and are isomorphous. The X-ray structural characterization of complexes **1**–**4** shows the presence of a discrete decameric water cluster built around a cyclic hexameric core stabilized by the solid-state structure, which represents another new mode of association of water molecules. The Ln^{3+}–Cr^{3+} magnetic interaction is negligible in **6** and **12**, antiferromagnetic in **2**, **4′**, **7**, **8**, **9**, **10**, and **11**, and unresolved for **3**. The complex **5** is a ferrimagnet because its magnetic studies suggest the onset of a very weak ferromagnetic three-dimensional ordering.

Introduction

Polycyanometalate complexes were employed as nodes in designing high-nuclearity complexes and coordination polymers with a rich variety of network topologies.[1] These studies mainly were focused on transition metals. Until now, great emphasis has been placed on magnetic studies of cyano-bridged transition metal assemblies. Some exciting results have been reported such as that some transition metal cyanides exhibit long-range magnetic ordering above room temperature.[2] The lanthanide cations have been less used as nodes for the construction of cyano-bridged heteropolymetallic coordination networks.[3] It is known that the f-block ions exhibit large and anisotropic magnetic moments and can form hard magnets when they are incorporated into the solids. In 1976, Hulliger et al. published a series of cyano-bridged three-dimensional (3D) rare earth hexacyanometalates (III) $[LnM(CN)_6]$·nH_2O (M = Fe or Cr, n = 4 or 5),[4] and ferrimagnetic ordering was observed in some of them. The incorporation of organic ligands as blocking ligands of the lanthanide ions reduces the dimensionality of the parent complexes and gives various molecular structures. To date, magnetic studies have been made for several cyano-bridged lanthanide transition metal complexes with different dimen-

* To whom correspondence should be addressed. E-mail: carme.diaz@qi.ub.es.

[†] Departament de Química Inorgànica, Universitat de Barcelona.

[‡] Departament de Cristal·lografia Mineralogia i Dipòsits Minerals, Universitat de Barcelona.

[#] University of Patras.

[§] Universidade da Coruña.

(1) (a) Ohba, M.; Õkawa, H. *Coord. Chem. Rev.* **2000**, *198*, 313. (b) Verdaguer, M.; Bleuzen, A.; Marvaud, V.; Vaissermann, J.; Seuleiman, M.; Desplanches, C.; Scuiller, A.; Train, C.; Garde, R.; Gelly, G.; Lomenech, C.; Rosenman, I.; Veillet, P.; Cartier, C.; Villain, F. *Coord. Chem. Rev.* **1999**, *190−192*, 1023. (c) Cernák, J.; Orendác, M.; Potonák, I.; Chomic, J.; Orendacová, A.; Skorsepa, J.; Feher, A. *Coord. Chem. Rev.* **2002**, *224*, 51.

(2) Holmes, S. M.; Girolami, G. S. *J. Am. Chem. Soc.* **1999**, *121*, 5593 and references therein.

(3) (a) Benelli, C; Gatteschi, D. *Chem. Rev.* **2002**, *102*, 2369. (b) de Sá, G. F.; Malta, O. P.; de Mello Donegá, C.; Simas, A. M.; Longo, R. L.; Santa-Cruz, P. A.; da Silva, E. F., Jr. *Coord. Chem. Rev.* **2000**, *196*, 165.

(4) Hulliguer, F.; Landolt, M.; Vetsch, H. *J. Solid State Chem.* **1976**, *18*, 283.

10.1021/ic060942q CCC: $33.50
Published on Web 09/06/2006

sionality: dinuclear,[5] trinuclear,[6] tetranuclear,[7] one-dimensional[6a,8] (1D), and two-dimensional[8e,9] (2D). In most cases, the magnetic properties of these complexes do not seem exciting, since the coupling between the lanthanide and transition metals is very weak because of the effective shielding of the 4f electrons by the outer-shell electrons. Important magnetic properties were found in only a few cyano-bridged rare earth transition metal complexes.[4,6a,8a,8e,8f,9a] With regard to polycyanometalates with the $[Cr(CN)_6]^{3-}$ ion acting as a bridged ligand, only a few systems have been reported containing lanthanide ions, such as (a) dinuclear systems $[Pr(DMF)_4(H_2O)_3Cr(CN)_6]\cdot H_2O$ (DMF = *N*,*N*-dimethylformamide),[10a] $[Dy(pyr)_4(H_2O)_3Cr(CN)_6]\cdot 2H_2O$ (pyr = 2-pyrrolidone),[10b] and $[Sm(DMSO)_4(H_2O)_3Cr(CN)_6]$ (DMSO = dimethyl sulfoxide);[10c] (b) tetranuclear system $[Gd(urea)_4(H_2O)_2]_2[Cr(CN)_6]_2$;[7a] (c) 1D systems $[CuL_2]_2Ln(H_2O)_2Cr(CN)_6\cdot 7H_2O$ (Ln^{3+} = Gd or La, L = dianion of 1,4,8,11-tetraazacyclotetradecane-2,3-dione),[11a] $[Nd(DMF)_4(H_2O)_2Cr(CN)_6]_n\cdot nH_2O$,[11b] $\{[Gd(capro)_2(H_2O)_4Cr(CN)_6]\cdot H_2O\}_n$ (capro = caprolactam),[7a] $[Sm(DMF)_4(H_2O)_2Cr(CN)_6]\cdot H_2O$,[8f] *cis*-$[Cr(CN)_4(\mu\text{-}CN)_2Gd(H_2O)_2(DMF)_4]_n\cdot nH_2O$, and *trans*-$[Cr(CN)_4(\mu\text{-}CN)_2Gd(H_2O)_4(bpy)]\cdot 4nH_2O\cdot 1.5n$bpy (bpy = 2,2′-bipyridine);[8b] (d) 2D systems $[Ln(DMF)_2(H_2O)_3\ Cr(CN)_6]\cdot H_2O$ (Ln^{3+} = Sm and Gd);[8f,9a] and (e) 3D systems of the formula $[LnCr(CN)_6]\cdot nH_2O$, which was reported by Hulliguer et al.[4]

On the basis of the literature, structural changes are found when using different building blocks, different solvents, and different stoichiometries, or when changing the specific lanthanide ion.[12−14] In general, when the same reactants and reaction conditions are used, only a few studies on the full lanthanide series are found. We are exploring a strategy to control the structure in the solid state that combines elements of design toward crystal engineering and the study of magnetic properties. We successfully applied this strategy in the preparation of a new species starting from the mononuclear species $[M(CN)_6]^{3-}$ (M = Fe^{3+}, Cr^{3+}, and Co^{3+}) as the building blocks, $Ln(NO_3)\cdot xH_2O$, and several different blocking ligands. With M = Fe^{3+} or Co^{3+} and *N*,*N*′-dimethylformamide (DMF) as the blocking ligand, we reported a family of 25 dinuclear complexes of formula the $[Ln(DMF)_4(H_2O)_3(\mu\text{-}CN)M(CN)_5]\cdot nH_2O$ (with Ln = all lanthanide(III) ions except Pm and Lu)[5b] using the same reaction conditions. Structural studies of these families show that they are isomorphous. When there are changes in the terminal blocking ligand, the structural types are modified such as in reactions involving Ln^{3+} ions, $[Co(CN)_6]^{3-}$ or $[Fe(CN)_6]^{3-}$, and using bpy instead of DMF as the terminal ligand. Therefore, an interesting feature appears. The early lanthanide ions of the series give trinuclear complexes of the formula *trans*-$[M(CN)_4(\mu\text{-}CN)_2\{Ln(H_2O)_4(bpy)_2\}_2][M(CN)_6]\cdot 8H_2O$,[6d] and when the series with the other lanthanide ions are completed, 1D structures of the formula *trans*-$[M(CN)_4(\mu\text{-}CN)_2Ln(H_2O)_4(bpy)]_n\cdot 4nH_2O\cdot 1.5n$bpy were found.[8a,8c] When the building block is $[Fe(CN)_6]^{3-}$, the Sm^{3+} ion is the limit of the trinuclear complexes. However, when the building block is $[Co(CN)_6]^{3-}$, the Nd^{3+} is the limit of the trinuclear complexes. Changes in the building block ligand also causes changes in the structural types. When $[Cr(CN)_6]^{3-}$, $Gd(NO_3)_3\cdot 6H_2O$, and DMF or bpy are used as the blocking ligand, two 1D complexes of the formula *cis*-$[Cr(CN)_4(\mu\text{-}CN)_2(DMF)Gd(H_2O)_2(DMF)_4]_n\cdot nH_2O$ and *trans*-$[Cr(CN)_4(\mu\text{-}CN)_2Gd(H_2O)_4(bpy)]_n\cdot 4nH_2O\cdot 1.5n$bpy are formed.[8b]

The present work is focused on the synthesis, characterization, and the study of the analogous magnetic properties of *trans*-$[Cr(CN)_4(\mu\text{-}CN)_2Gd(H_2O)_4(bpy)]_n\cdot 4n$H2O·1.5*n*bpy, which previously were described by us[8b] using all the lanthanide(III) ions. From the early lanthanide ions, 1D systems of the formula *trans*-$[Cr(CN)_4(\mu\text{-}CN)_2Ln(H_2O)_3(bpy)_2]_n\cdot 4nH_2O\cdot 3.5n$bpy ($Ln^{3+}$ = La, Ce, Pr, Nd) were obtained. With the other lanthanide ions as well as the Nd^{3+} ion, 1D complexes of the formula *trans*-$[Cr(CN)_4(\mu\text{-}CN)_2Ln(H_2O)_4(bpy)]_n\cdot 3.5nH_2O\cdot 1.5n$bpy ($Ln^{3+}$ = Nd, Sm, Eu, Tb, Dy, Ho, Er, Tm, Yb, and Lu) were obtained. All these complexes show a 3D supramolecular structure built by an intricate array of hydrogen bonds involving contributions from the coordination and the crystallization of water molecules with the most notable being a water decamer $(H_2O)_{10}$ for the first family of these complexes.

Structural investigation of water molecules has received considerable interest, because water is fundamental for life,

(5) (a) Gao S.; Ma, B.; Wang, Z.; Yi, T.; Liao, C.; Yan, C.; Xu, G. *Mol. Cryst. Liq. Cryst. Sci. Technol., Sect. A* **1999**, *335*, 201. (b) Figuerola, A.; Diaz, C., Ribas, J.; Tangoulis, V.; Granell, J.; Lloret, F.; Mahía, J.; Maestro, M. *Inorg. Chem.* **2003**, *42*, 641. (c) Sun, X. R.; Chen, Z. D.; Yan, F.; Gao, S.; Cheung, K. K.; Che, C. M.; Zhang, X. X. *J. Cluster Sci.* **2002**, *13*, 103.

(6) (a) Yan, B.; Chen, Z. *Helv. Chim. Acta* **2001**, *84*, 817. (b) Yan, B.; Chen, Z. *Chem. Lett.* **2000**, *11*, 1244. (c) Yi, T.; Gao, S.; Chen, X. W.; Yan, C. H.; Li, B. G. *Acta Crystallogr.* **1998**, *C54*, 41. (d) Figuerola, A.; Ribas, J.; Llunell, M.; Casanova, D.; Maestro, M.; Alvarez, S.; Diaz, C. *Inorg. Chem.* **2005**, *44*, 6939.

(7) (a) Kou, H. Z.; Gao, S.; Li, C. H.; Liao, D. Z.; Zhou, B. C.; Wang, R. J.; Li, Y. *Inorg. Chem.* **2002**, *41*, 4756. (b) Gao, S.; Ma, B. Q.; Sun, H. L.; Li, J. R. *J. Solid State Chem.* **2003**, *171*, 201.

(8) (a) Figuerola, A.; Diaz, C.; Ribas, J.; Vassilis, T.; Sangregorio, C.; Gatteschi, D.; Maestro, M.; Mahía, J. *Inorg. Chem.* **2003**, *42*, 5274. (b) Figuerola, A.; Diaz, C.; El Fallah, M. S.; Ribas, J.; Maestro, M.; Mahía, J. *Chem. Commun.* **2001**, 1204. (c) Figuerola, A.; Ribas, J.; Casanova, D.; Maestro, M.; Alvarez, S.; Diaz, C. *Inorg. Chem.* **2005**, *44*, 6949. (d) Yan, B.; Wang, H. D.; Chen, Z. D. *Polyhedron* **2001**, *20*, 591. (e) Yan, B.; Chen, Z.; Wang, S.; Gao, S. *Chem Lett.* **2001**, 350. (f) Kou, H. Z.; Gao, S.; Jin, X. *Inorg. Chem.* **2001**, *40*, 6295. (g) Shi, W.; Chen, X. Y.; Zhao, B.; Yu, A.; Song, H. B.; Cheng, P.; Wang, H. G. *Inorg. Chem.* **2006**, *45*, 3949.

(9) (a) Kou, H. Z.; Gao, S.; Sun, B. W.; Zhang, J. *Chem. Mater.* **2001**, *13*, 1431. (b) Zhao, Q. H.; Wang, Q. H.; Fang, R. B. *Trans. Met. Chem.* **2004**, *29*, 144. (c) Ma, B. Q.; Gao, S.; Su, G.; Xu, G. X. *Angew. Chem. Int. Ed.* **2001**, *40*, 434.

(10) (a) Combs, R. A.; Farmer, J. M.; Kautz, J. A. *Acta Crystallogr.* **2000**, *C56*, 1420. (b) Kou, H. Z.; Gao, S.; Wang, R. J. *Acta Crystallogr.* **2002**, *C58*, m325. (c) Zhou, B. C.; Kou, H. Z.; He, Y.; Wang, R. J.; Li, Y. D.; Wang, H. G. *Chin. J. Chem.* **2003**, *21*, 352.

(11) (a) Kou, H. Z.; Zhou, B. C.; Wang, R. J. *Inorg. Chem.* **2003**, *42*, 7658. (b) Kou, H.; Gao, S.; Sun, B; Ma, B. *Acta Sci. Nat.* **2001**, *37*, 261.

(12) (a) Blake, A. J.; Gould, R. O.; Grant, C. M.; Milne, P. E.; Parson, S.; Winpenny, R. E. P. *J. Chem. Soc., Dalton Trans.* **1997**, 485 and references therein. (b) Blake, A. J.; Milne, P. E. Y. Winpenny, R. E. P. *J. Chem. Soc., Dalton Trans.* **1993**, 3727. (c) Benelli, C.; Blake, A. J.; Milne, P. E. Y.; Rawson, J. M.; Winpenny, R. E. P. *Chem.—Eur. J.* **1995**, *9*, 614.

(13) (a) Cui, Y. C.; Chen, J. T.; Ren, J.; Kian, Y.; Huang, J. S. *Inorg. Chem.* **2000**, *39*, 4165. (b) Cui, Y. C.; Chen, J. T.; Long, D. L.; Zheng, F. K.; Cheng, W. D.; Huang, J. S. *J. Chem. Soc., Dalton Trans.* **1998**, 2955.

(14) Gheorghe, R.; Cucos, P.; Andruh, M.; Costes, J. P.; Donnadieu, B.; Soba, S. *Chem.—Eur. J.* **2006**, *12*, 187.

and it plays an important role in many biological and chemical systems.[15] Hydrogen-bonded $(H_2O)_n$ clusters can play an important role in the stabilization of some supramolecular species, which are both natural and synthetic, in an aqueous solution. Theoretical calculations[15,16] on "isolate" small water clusters $(H_2O)_n$ ($n = 6-12$) indicate that there are several essentially isoenergetic isomers for a given water cluster and that the lowest energy isomer possesses the maximum number of hydrogen bonds. Some interesting polymeric water phases consisting of basic water tetramer, pentamer, and hexamer subunits have been reported.[17,18] Some examples of different topologies with the focus on the $(H_2O)_{10}$ cluster are found in the literature.[19−23]

Experimental Section

Materials. All starting materials were purchased from Aldrich and were used without further purification. The analogous *trans*-$[Co(CN)_4(\mu\text{-}CN)_2Ln(H_2O)_4(bpy)]_n \cdot 4nH_2O \cdot 1.5n$bpy complexes previously reported by us were prepared according to the literature method.[8c]

Synthesis of the New Complexes. ***trans*-[Cr(CN)$_4$(μ-CN)$_2$La(H$_2$O)$_3$(bpy)$_2$]$_n$·4*n*H$_2$O·3.5*n*bpy (1), *trans*-[Cr(CN)$_4$(μ-CN)$_2$Ce(H$_2$O)$_3$(bpy)$_2$]$_n$·4*n*H$_2$O·3.5*n*bpy (2), *trans*-[Cr(CN)$_4$(μ-CN)$_2$Pr(H$_2$O)$_3$(bpy)$_2$]$_n$·4*n*H$_2$O·3.5*n*bpy (3), *trans*-[Cr(CN)$_4$(μ-CN)$_2$ Nd(H$_2$O)$_3$(bpy)$_2$]$_n$·4*n*H$_2$O·3.5*n*bpy (4), *trans*-[Cr(CN)$_4$(μ-CN)$_2$Nd(H$_2$O)$_4$(bpy)]$_n$·3.5*n*H$_2$O ·1.5*n*bpy (4′), *trans*-[Cr(CN)$_4$(μ-CN)$_2$Sm(H$_2$O)$_4$(bpy)]$_n$·3.5*n*H$_2$O·1.5*n*bpy (5), *trans*-[Cr(CN)$_4$(μ-CN)$_2$Eu(H$_2$O)$_4$(bpy)]$_n$·3.5*n*H$_2$O·1.5*n*bpy (6), *trans*-[Cr(CN)$_4$(μ-CN)$_2$Tb(H$_2$O)$_4$(bpy)]$_n$·3.5*n*H$_2$O·1.5*n*bpy (7), *trans*-[Cr(CN)$_4$(μ-CN)$_2$Dy(H$_2$O)$_4$(bpy)]$_n$·3.5*n*H$_2$O ·1.5*n*bpy (8), *trans*-[Cr(CN)$_4$(μ-CN)$_2$Ho(H$_2$O)$_4$(bpy)]$_n$·3.5*n*H$_2$O·1.5*n*bpy (9), *trans*-[Cr(CN)$_4$(μ-CN)$_2$Er(H$_2$O)$_4$(bpy)]$_n$·3.5*n*H$_2$O·1.5*n*bpy (10), *trans*-[Cr(CN)$_4$(μ-CN)$_2$Tm(H$_2$O)$_4$(bpy)]$_n$·3.5*n*H$_2$O·1.5*n*bpy (11), *trans*-[Cr(CN)$_4$(μ-CN)$_2$Yb(H$_2$O)$_4$(bpy)]$_n$·3.5*n*H$_2$O·1.5*n*bpy (12) and *trans*-[Cr(CN)$_4$(μ-CN)$_2$Lu(H$_2$O)$_4$(bpy)]$_n$·3.5*n*H$_2$O·1.5*n*bpy (13).** All the complexes were obtained by adding a solution of $Ln(NO_3)_3 \cdot nH_2O$ ($n = 5$, 6) (1.1 mmol) in water (25 mL) to an equimolar solution of $K_3[Cr(CN)_6]$ in water (25 mL). To this mixture, an ethanolic solution (5 mL) of bpy (3.3 mmol) was added. The solution was left undisturbed, and well-formed crystals were obtained after several days (**1**, orange; **3**, yellow-green; and **2**, **4**−**13**, yellow) (yields 60−70%). In the syntheses of complex **4**, the elemental analysis was not consistent with a well-characterized product, and the repetition of the synthetic method gave different analytical results. These results implied the simultaneous synthesis of different kinds of products. The crystals that were obtained were of the same color and morphology, but, fortunately, we were able to structurally characterize the two products (**4** and **4′**) of the mixture. We obtained complex **4** with high purity in one attempt, and this allowed us to study their magnetic behavior. Complex **4′** was the minority product. Anal. Calcd for **1** ($C_{61}H_{58}CrLaN_{17}O_7$): C, 55.00; N, 17.87; H, 4.38. Found: C, 55.1; N, 17.9; H, 4.3. Anal. Calcd for **2** ($C_{61}H_{58}CrCeN_{17}O_7$): C, 54.95; N, 17.86; H, 4.38. Found: C, 55.0; N, 17.9; H, 4.3. Anal. Calcd for **3** ($C_{61}H_{58}CrN_{17}O_7Pr$): C, 54.92; N, 17.85; H, 4.38. Found: C, 54.8; N, 17.9; H, 4.4. Anal. Calcd for **4** ($C_{61}H_{58}CrN_{17}NdO_7$): C, 54.78; N, 17.80; H, 4.37. Found: C, 54.7; N, 17.77; H, 4.2. Anal. Calcd for **5** ($C_{31}H_{35}CrN_{11}O_{7.5}Sm$): C, 42.12; N, 17.43; H, 3.99. Found: C, 42.1; N, 17.4; H, 3.9. Anal. Calcd for **6** ($C_{31}H_{35}CrEuN_{11}O_{7.5}$): C, 42.04; N, 17.40; H, 3.98. Found: C, 42.1; N, 17.4; H, 4.1. Anal. Calcd for **7** ($C_{31}H_{35}CrN_{11}O_{7.5}Tb$): C, 41.71; N, 17.26; H, 3.95. Found: C, 41.5; N, 17.1; H, 4.0. Anal. Calcd for **8** ($C_{31}H_{35}CrDyN_{11}O_{7.5}$): C, 41.55; N, 17.19; H, 3.93. Found: C, 41.5; N, 17.3; H, 3.9. Anal. Calcd for **9** ($C_{31}H_{35}CrHoN_{11}O_{7.5}$): C, 41.43; N, 17.14; H, 3.92. Found: C, 41.4; N, 17.0; H, 4.1. Anal. Calcd for **10** ($C_{31}H_{35}CrErN_{11}O_{7.5}$): C, 41.32; N, 17.10; H, 3.91. Found: C, 41.3; N, 17.2; H, 4.0. Anal. Calcd for **11** ($C_{31}H_{35}CrN_{11}O_{7.5}Tm$): C, 41.25; N, 17.07; H, 3.91. Found: C, 41.2; N, 17.1; H, 4.0. Anal. Calcd for **12** ($C_{31}H_{35}CrN_{11}O_{7.5}Yb$): C, 41.06; N, 16.99; H, 3.89. Found: C, 41.2; N, 17.0; H, 4.1. Anal. Calcd for **13** ($C_{31}H_{35}CrLuN_{11}O_{7.5}$): C, 40.97; N, 16.96; H, 3.88. Found: C, 41.0; N, 17.1; H, 4.0.

Crystal Structure Determination. Crystal data and details on the data collection and refinement are summarized in Tables 1−3. The crystal data for complexes **1**−**4**, **4′**, **6**−**11**, and **13** were collected using a MAR345 diffractometer with an image plate detector. For complexes **5** and **12,** data were collected using a Bruker SMART-CCD area diffractometer. Intensities were collected with graphite-monochromatized Mo−K α-radiation. The refinement method employed was full-matrix least-squares on F^2. The results of the integration process are summarized in Tables 1−3. The structures were solved by direct methods using the SHELXS computer program[24] and were refined by the full-matrix least-squares method with the SHELX97 computer program.[24]

For complexes **1**−**4**, several crystals were measured, and the best refinement obtained from the data collection is presented. For complexes **1**−**4**, the crystallization of bipyridine (N22, N23) was located on a mirror plane, and the N atoms have been assumed in disorder sites with an occupancy factor of 0.5.

The number of hydrogen atoms computed was 40 for **1**, 39 for **2**, 40 for **3**, 40 for **4**, 22 for **4′**, 31 for **5**, 24 for **6**, 20 for **7**, 33 for **8**, 29 for **9**, 33 for **10**, 33 for **11**, 31 for **12**, and 20 for **13**. The water hydrogen atoms could not be located except in complexes **5** and **12** in which the atoms were located from a difference synthesis. All hydrogen atoms were refined using a riding model with the exception of **11**, which were refined freely.

Physical Measurements. Magnetic measurements were carried out in the "Servei de Magnetoquímica (Universitat de Barcelona)" on polycrystalline samples (20 mg) with a Quantum Design SQUID MPMS-XL magnetometer working in the 2−300 K range. The magnetic field was 8000 Gauss. The field-dependent magnetization was measured in the applied magnetic field range of 0−5 T at 2 K. The diamagnetic corrections were evaluated from Pascal's constants.

Results and Discussion

Fourteen $[CrLn]_n$ 1D complexes were synthesized in the same manner (Scheme 1). Their formulas are *trans*-$[Cr(CN)_4$-

(15) Ludwing, R. *Angew. Chem., Int. Ed*. **2001**, *40*, 1808 and references therein.
(16) (a) Kim, J.; Kim, K. S. *J. Chem. Phys*. **1998**, *109*, 5886. (b) Kim, J.; Majumbur, D.; Lee, H. M.; Kim, K. S. *J. Chem Phys*. **1999**, *110*, 9128. (c) Prasad, T. K.; Rajasekharan, M. V. *Cryst. Growth Des*. **2006**, *6*, 488. (d) Bruck, U.; Ettischer, I.; Melzer, M.; Buch, V.; Sadlej J. *Phys Rev. Lett*. **1998**, *80*, 2578.
(17) Pal, S.; Sankaran, N. B.; Samanta, A. *Angew. Chem., Int. Ed*. **2003**, *42*, 1741. (b) Ma, B. Q.; Sun, H. L.; Gao, S. *Chem. Commun*. **2004**, 2220.
(18) Custelcean, R.; Afloroaei, C.; Vlassa, M.; Polverejan, M. *Angew. Chem., Int. Ed*. **2000**, *39*, 3094.
(19) Neogi, S.; Bharadwaj, P. K. *Cryst. Growth Des*. **2006**, *6*, 433.
(20) Mukhopadhyay, U.; Bernal, I. *Cryst. Growth Des*. **2006**, *6*, 363.
(21) Barbour, L. J.; Orr, G. W.; Atwood, J. L. *Nature* **1998**, *393*, 671.
(22) Li, Y.; Jiang, L.; Feng, X. L.; Lu, T. B. *Cryst. Growth Des.* **2006**, *6*, 1074.
(23) Barbour, L. J.; Orr, G. W.; Atwood, J. L. *Chem. Commun*. **2000**, 859.
(24) Sheldrick, G. M. *A Computer Program for Determination of Crystal Structure;* University Göttingen, Germany, 1997.

Table 1. Crystal Parameters for **1**−**4**

	1	**2**	**3**	**4**
empirical formula	$C_{61}H_{58}CrLaN_{17}O_7$	$C_{61}H_{58}$ $CeCrN_{17}O_7$	$C_{61}H_{58}$ $CrN_{17}PrO_7$	$C_{61}H_{58}CrN_{17}NdO_7$
formula mass	1332.15	1333.36	1334.15	1337.48
crystal size (mm^3)	0.50 × 0.50 × 0.18	0.40 × 0.30 × 0.19	0.35 × 0.25 × 0.15	0.42 × 0.31 × 0.12
crystal color	orange	yellow	yellow-green	yellow
crystal system	orthorhombic	orthorhombic	orthorhombic	orthorhombic
space group	*Pbam*	*Pbam*	*Pbam*	*Pbam*
Z	8	8	8	8
a (Å)	25.522(4)	25.396(6)	25.419(8)	25.429(3)
b (Å)	20.962(10)	20.883(5)	20.927(6)	20.990(5)
c (Å)	22.9678(10)	22.885(8)	22.805(9)	22.831(4)
α (deg)	90	90	90	90
β (deg)	90	90	90	90
γ (deg)	90	90	90	90
V ($Å^3$)	12287(8)	12137(6)	12131(7)	12186(4)
ρ (calc) (g/cm^3)	1.439	1.458	1.460	1.457
μ_{calc} (mm^{-1})	0.930	0.987	1.040	1.088
T (K)	203(2)	203(2)	203(2)	203(2)
F (000)	5440	5448	5456	5464
Θ range for data collection	1.54−31.62	3.40−31.71	1.83−32.45	1.54−32.19
total reflns	42429	65433	80240	70412
independent reflns [R(int)]	12038 [0.053]	15394 [0.123]	18476 [0.173]	16939 [0.074]
reflns $I > 2\sigma(I)$	10802	14595	11616	15129
params refined, restraints	796, 27	828, 27	796, 27	797, 27
final *R* indices[a]	R1 = 0.0684	R1 = 0.0411	R1 = 0.1153	R1 = 0.0754
[$I > 2\sigma(I)$]	wR2 = 0.1626	wR2 = 0.1018	wR2 = 0.2364	wR2 = 0.1686
final wR2 indices[a]	R1 = 0.0747	R1 = 0.0491	R1 = 0.1986	R1 = 0.0822
(all data)	wR2 = 0.1663	wR2 = 0.1095	wR2 = 0.2731	wR2 = 0.1718
largest diff peak, hole (e $Å^{-3}$)	1.466, −0.760	0.747, −0.497	1.290, −1.651	1.786, −1.176
weights (a,b)[b]	0.0424, 89.064	0.0175, 18.6087	0.0739, 38.5534	0.0309, 75.5503

[a] $R1 = \sum||F_0|^2 - |F_c|^2|$ and $wR2 = \{\sum(F_0^2 - F_c^2)/\sum w(F_0^2)\}^{1/2}$. [b] The weighting scheme employed was $w = [\sigma^2(I) + (aP)^2 + bP]^{-1}$ and $P = (|F_0^2| + 2|F_c^2|)/3$. *f*, *f′*, and *f″* were taken from International Tables of X-ray Crystallography.[25]

Table 2. Crystal Parameters for **4′**−**8**

	4′	**5**	**6**	**7**	**8**
empirical formula	$C_{31}H_{35}CrN_{11}NdO_{7.5}$	$C_{31}H_{35}CrN_{11}O_{7.5}Sm$	$C_{31}H_{35}CrEuN_{11}O_{7.5}$	$C_{31}H_{35}CrTbN_{11}O_{7.5}$	$C_{31}H_{36}CrDyN_{11}O_{7.5}$
formula mass	877.91	884.03	885.64	892.60	896.18
crystal size (mm^3)	0.35 × 0.30 × 0.10	0.50 × 0.20 × 0.19	0.28 × 0.24 × 0.09	0.38 × 0.27 × 0.13	0.25 × 0.22 × 0.10
crystal color	yellow	yellow	yellow	yellow	yellow
crystal system	triclinic	triclinic	triclinic	triclinic	triclinic
space group	*P*$\bar{1}$	*P*$\bar{1}$	*P*$\bar{1}$	*P*$\bar{1}$	*P*$\bar{1}$
Z	2	2	2	2	2
a (Å)	9.854(4)	9.8649(7)	9.862(4)	9.839(4)	9.828(4)
b (Å)	10.858(3)	10.8552(7)	10.840(3)	10.789(4)	10.773(3)
c (Å)	19.806(5)	19.9156(13)	19.917(6)	19.776(7)	19.806(6)
α (deg)	83.34(2)	83.413(1)	83.41(2)	83.54(2)	83.61(2)
β (deg)	83.31	83.682(1)	83.77(2)	83.88(2)	84.01(2)
γ (deg)	65.48(2)	65.266(1)	65.02(2)	64.95(2)	64.88(2)
V ($Å^3$)	1909.5(11)	1919.7(2)	1913.0(11)	1885.7(12)	1883.1(11)
ρ (calc) (g/cm^3)	1.528	1.548	1.538	1.573	1.581
μ_{calc} (mm^{-1})	1.689	1.858	1.967	2.208	2.317
T (K)	203(2)	203(2)	203(2)	203(2)	203(2)
F (000)	884	888	890	896	896
Θ range for data collection	3.72−28.22	2.06−28.28	3.60−29.13	3.75−27.73	3.62−29.51
total reflns	11542	12395	11129	9284	13323
independent reflns [*R*(int)]	6539 [0.029]	8711 [0.0235]	6591 [0.031]	5675 [0.043]	7269 [0.027]
reflns $I > 2\sigma(I)$	6353	8711	6332	5508	7016
params refined	524	489	532	488	550
final *R* indices[a]	R1 = 0.0456	R1 = 0.0266	R1 = 0.0331	R1 = 0.0343	R1 = 0.0200
[$I > 2\sigma(I)$]	wR2 = 0.1409	wR2 = 0.0681	wR2 = 0.0988	wR2 = 0.1134	wR2 = 0.0492
params refined, restraints	524, 0	489, 0	532, 0	488, 0	550, 0
final wR2 indices[a]	R1 = 0.0480	R1 = 0.0317	R1 = 0.0357	R1 = 0.0377	R1 = 0.0217
(all data)	wR2 = 0.1513	wR2 = 0.0700	wR2 = 0.1040	wR2 = 0.1316	wR2 = 0.0506
largest diff peak, hole (e $Å^{-3}$)	0.668, −0.521	0.822, −1.234	0.967, −1.142	0.466, −0.619	0.472, −0.600
weights (a,b)[b]	0.0975, 2.3133	0.0334, 0.1043	0.0451, 5.2630	0.0655, 6.7333	0.0202, 2.0283

[a] $R1 = \sum||F_0|^2 - |F_c|^2|$ and $wR2 = \{\sum w(F_0^2 - F_c^2)/\sum w(F_0^2]\}^{1/2}$. [b] The weighting scheme employed was $w = [\sigma^2(I) + (aP)^2 + bP]^{-1}$ and $P = (|F_0^2| + 2|F_c^2|)/3$. *f*, *f′* and *f″* were taken from International Tables of X-ray Crystallography.[25]

$(\mu\text{-}CN)_2Ln(H_2O)_3(bpy)_2]_n \cdot 4nH_2O \cdot 3.5n$bpy for the early lanthanide(III) ions (La−Nd) and *trans*-$[Cr(CN)_4(\mu\text{-}CN)_2Ln(H_2O)_4(bpy)]_n \cdot 3.5nH_2O \cdot 1.5n$bpy for the other ions (Sm−Lu as well as Nd).

Table 3. Crystal Parameters for **9**−**13**

	9	**10**	**11**	**12**	**13**
empirical formula	$C_{31}H_{35}CrHoN_{11}O_{7.5}$	$C_{31}H_{35}CrErN_{11}O_{7.5}$	$C_{31}H_{35}CrTmN_{11}O_{7.5}$	$C_{31}H_{35}CrYbN_{11}O_{7.5}$	$C_{31}H_{35}CrLuN_{11}O_{7.5}$
formula mass	898.60	900.94	902.61	906.72	908.64
crystal size (mm^3)	0.38 × 0.25 × 0.11	0.36 × 0.22 × 0.13	0.24 × 0.18 × 0.14	0.50 × 0.19 × 0.09	0.22 × 0.11 × 0.10
crystal color	yellow	yellow	yellow	yellow	yellow
crystal system	triclinic	triclinic	triclinic	triclinic	triclinic
space group	$P\bar{1}$	$P\bar{1}$	$P\bar{1}$	$P\bar{1}$	$P\bar{1}$
Z	2	2	2	2	2
a (Å)	9.805(4)	9.840(4)	9.812(4)	9.8332(15)	9.804(4)
b (Å)	10.745(3)	10.767(3)	10.735(3)	10.7618(16)	10.710(3)
c (Å)	19.749(7)	19.780(6)	19.753(6)	19.901(3)	19.795(6)
α (deg)	83.88(2)	83.64(2)	83.61(2)	83.596(3)	83.67(2)
β (deg)	83.02(2)	84.15(2)	84.18(2)	84.282(3)	84.38(2)
γ (deg)	64.85(2)	64.59(2)	64.63(2)	64.463(2)	64.46(2)
V ($Å^3$)	1865.9(11)	1877.8(11)	1865.0(11)	1885.3(5)	1861.0
ρ (calc) (g/cm^3)	1.600	1.594	1.608	1.617	1.622
μ_{calc} (mm^{-1})	2.456	2.569	2.715	2.815	2.990
T (K)	203(2)	203(2)	203(2)	203(2)	203(2)
F (000)	898	900	902	904	906
Θ range for data collection	3.66−31.89	3.62−30.12	3.63−31.86	2.06−28.25	3.63−27.38
total reflns	15862	13617	14772	12134	10216
independent reflns [R(int)]	8758 [0.030]	7434 [0.025]	8382 [0.028]	8528 [0.0239]	5917 [0.040]
reflns $I > 2\sigma(I)$	8330	7194	7985	7650	5747
params refined	604	619	619	489	488
final R indices[a]	R1 = 0.0222	R1 = 0.0210	R1 = 0.0251	R1 = 0.0295	R1 = 0.0268
[$I > 2\sigma(I)$]	wR2 = 0.0580	wR2 = 0.0686	wR2 = 0.0659	wR2 = 0.0711	wR2 = 0.0841
params refined, restraints	604, 0	619, 0	619, 0	489, 0	488, 0
Final wR2 indices[a]	R1 = 0.0254	R1 = 0.0232	R1 = 0.0282	R1 = 0.0350	R1 = 0.0294
(all data)	wR2 = 0.0612	wR2 = 0.0818	wR2 = 0.0726	wR2 = 0.0733	wR2 = 0.0886
largest diff peak, hole (e $Å^{-3}$)	0.786, −0.514	0.802, −0.820	0.505, −0.527	1.197, −1.743	0.748, −0.756
weights (a,b)[b]	0.0162, 3.8079	0.0455, 4.8534	0, 8.6498	0.0390, 0	0.0473, 4.5047

[a] $R1 = \sum||F_0|^2 - |F_c|^2|$ and $wR2 = \{\sum w(F_0^2 - F_c^2)/\sum w(F_0^2]\}^{1/2}$. [b] The weighting scheme employed was $w = [\sigma^2(I) + (aP)^2 + bP]^{-1}$ and $P = (|F_0^2| + 2|F_c^2|)/3$. f, f' and f'' were taken from International Tables of X-ray Crystallography.[25]

Scheme 1

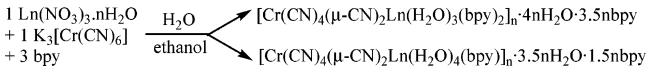

Description of the Structures of Complexes 1−13. The structure of the 14 complexes consists of a 1D polymer. Complexes **1**−**4** are isomorphous and crystallize in the orthorhombic system, and the space group is *Pbam*. Complexes **4′**−**13** also are isomorphous, crystallize in the triclinic system, and the space group is $P\bar{1}$. An ORTEP view of **4** and **4′** with the atom-labeling scheme are represented in Figures 1a and 2a, respectively. Selected bond lengths and angles for **1**−**4** and **4′**−**13** are listed in Tables 4 and 5, respectively.

The crystallographic analysis of complexes **1**−**4** revealed that they all confine isomorphous 1D polymers. As an example, the structure of **1** is shown in Figure 1b. The chain is made by the cyano-bridged alternating $Cr1(CN)_6$-Ln-$(H_2O)_3(bpy)_2$-$Cr2(CN)_6$ fragment (Ln^{3+} = La, Ce, Pr, and Nd) and rungs along the z axes. The Ln^{3+} is a nine-coordinated ion with three oxygen atoms of three water molecules, four nitrogen atoms of two bpy ligands, and two nitrogen atoms of the cyanide bridges. The longest Ln−O and Ln−N distances correspond to the La^{3+} ion and the shortest ones correspond to the Nd^{3+} ion in accordance with the variation of the radius of the lanthanide ions. Six cyanide ligands surround the Cr^{3+} ion in a distorted octahedral environment. Each $[Cr(CN)_6]$ fragment coordinates to two Ln^{3+} ions using two trans cyanide ligands (Figure 1b). The

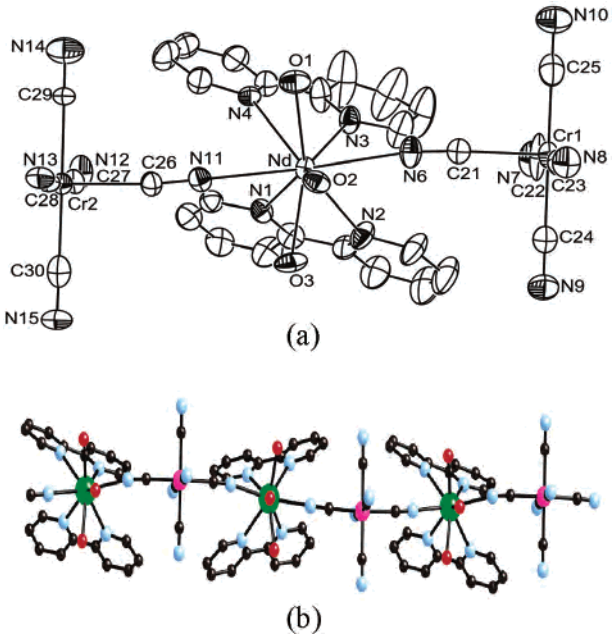

Figure 1. (a) ORTEP view of complex **4** with atom-labeling scheme (ellipsoids drawn at 50% probability level). Complexes **1**−**3** show a similar structure (they are isostructural). (b) Schematic representation of the chain.

Ln−Cr1 and Ln−Cr2 distances are 5.886 and 5.888 Å for **1**, 5.868 and 5.866 Å for **2**, 5.853 and 5.839 Å for **3**, and 5.853 and 5.848 Å for **4**, respectively. The Cr1−Ln−Cr2, Ln−Cr1−Ln, and Ln−Cr2−Ln angles are 156.79, 156.92, and 152.26° for **1**, 156.73, 156.90, and 152.18° for **2**, 156.61,

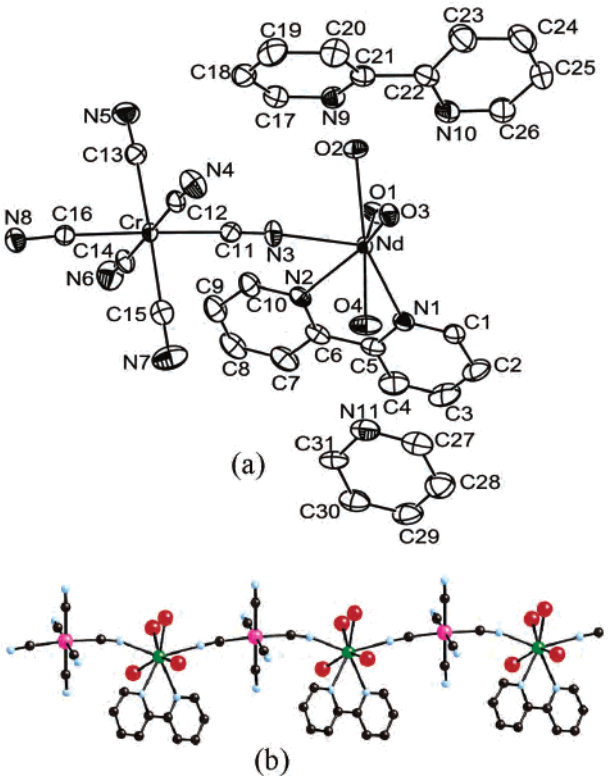

Figure 2. (a) ORTEP view of complex **4′** with atom-labeling scheme (ellipsoids drawn at 50% probability level). Complexes **5**−**13** show a similar structure (they are isostructural). (b) Schematic representation of the chain.

156.93, and 152.10° for **3**, and 156.83, 156.95, and 152.56° for **4**, respectively.

Their supramolecular structures are created by hydrogen bonding. The chains are self-assembled through hydrogen bonds in very different pathways because of the high number of atoms that could participate with them. Some of the different pathways and number of atoms of the four isomorphous complexes involved in the 3D self-assembled structure through hydrogen bonds are shown in Figure 3a−c for **1**. All the oxygen atoms (O1W−O8W) of the water molecules of crystallization, the O1, O2, and O3 oxygen atoms of the coordinated water molecules to the lanthanide ion, and all the nitrogen atoms of the cyanide terminal ligands and one of the bpy molecules of crystallization (N20−N21) participate in the supramolecular structure giving it an extensive 3D network. The bpy molecules of crystallization (except N22−N23) adopt different stereo configurations because of the presence of hydrogen bonds (Figure 3a−c). The bpy molecules of crystallization are not planar, thus showing dihedral angles: (N20−N21) of 177.68 for **1**, 179.05 for **2**, 175.13 for **3**, and 179.9 for **4**; (N18−N19) of 23.34 for **1**, 26.47 for **2**, 24.27 for **3**, and 29.26 for 4; and (N16−N17) of 36.50 for **1**, 35.35 for **2**, 36.10 for **3**, and 34.62 for 4. The 3D supramolecular structure involves the contribution from the discrete $(H_2O)_{10}$ built around a cyclic hexameric core with an inversion center in the middle of the ring (Figure 4a), which represent a new mode of association of water molecules. In the decamer, the OW−OW distances are in the range of 2.72−2.92 Å. The hexameric core forms a quasi-planar ring. Four water molecules (O1W and O3W) of each

Table 4. Selected Bonds Lengths (Å) and Angles (deg) for **1**−**4**

	1	**2**	**3**	**4**
Ln−O(1)	2.495(4)	2.461(2)	2.434(6)	2.430(4)
Ln−O(2)	2.540(4)	2.511(2)	2.491(5)	2.469(3)
Ln−O(3)	2.488(5)	2.458(2)	2.444(6)	2.421(4)
Ln−N(1)	2.721(4)	2.698(3)	2.694(7)	2.663(4)
Ln−N(2)	2.803(5)	2.762(2)	2.750(7)	2.726(4)
Ln−N(3)	2.769(5)	2.746(3)	2.705(7)	2.719(4)
Ln−N(4)	2.771(5)	2.744(3)	2.733(7)	2.735(4)
Ln−N(6)	2.703(5)	2.680(3)	2.636(6)	2.640(4)
Ln−N(11)	2.690(5)	2.649(3)	2.641(6)	2.640(4)
Cr(1)−C(21)	2.104(6)	2.099(3)	2.086(8)	2.109(5)
Cr(1)−C(22)	2.046(9)	2.058(4)	2.060(12)	2.045(8)
Cr(1)−C(23)	2.102(9)	2.103(4)	2.068(13)	2.090(7)
Cr(1)−C(24)	2.060(11)	2.108(5)	2.163(16)	2.070(8)
Cr(1)−C(25)	2.052(11)	2.098(5)	2.112(16)	2.059(10)
Cr(2)−C(26)	2.092(6)	2.092(3)	2.055(8)	2.097(5)
Cr(2)−C(27)	2.073(9)	2.079(4)	2.114(12)	2.063(7)
Cr(2)−C(28)	2.089(9)	2.065(4)	2.086(13)	2.077(8)
Cr(2)−C(29)	2.091(12)	2.121(7)	2.11(2)	2.122(6)
Cr(2)−C(30)	2.096(11)	2.142(5)	2.078(13)	2.121(10)
N(6)−C(21)	1.127(8)	1.131(4)	1.177(9)	1.147(6)
N(11)−C(26)	1.154(8)	1.167(4)	1.181(10)	1.158(6)
C(21)−N(6)−Ln	168.7(5)	170.8(3)	170.2(7)	171.4(5)
C(26)−N(11)−Ln	175.1(4)	174.6(2)	173.7(6)	175.6(4)
N(6)−C(21)−Cr(1)	173.3(4)	172.9(2)	172.4(7)	171.8(4)
N(11)−C(26)−Cr(2)	168.6(5)	170.0(2)	171.4(7)	168.1(4)

decameric cluster are bound to the host lattice through hydrogen bonds with six nitrogen atoms of one of the terminal cyanide ligands of six different chains at distances of around 3 Å (Figure 4b). Thus, it appears that the water clusters act as a template around the pack of the chains. The bpy ligand (N22−N23) and $(H_2O)_{10}$ occupy cavities of the crystal in the *z* direction (Figure 4c). Hydrogen bond distances are shown for complexes **1**−**4** (Supporting Information, Table S1). The bpy of crystallization (N20−N21) and the bpy ligands of the chains exhibit a weak $\pi-\pi$ interaction giving a supramolecular bidimensional structure (Figure 3d). Intermolecular stacking distances between centroids of the bpy rings are shown for complexes **1**−**4** in Table 6. These $\pi-\pi$ interactions provide additional stabilization of the crystal structure.

For complexes **4′**−**13**, the chain is made by the cyano-bridged alternating $Cr(CN)_6$-$Ln(H_2O)_4$(bpy) fragment. The Ln^{3+} ions are eight-coordinated with four oxygen atoms from the four water molecules, two nitrogen atoms from the bpy ligand, and two nitrogen atoms from the cyanide bridges. The longest Ln−O and Ln−N distances correspond to the Nd^{3+} ion and the shortest ones correspond to the Lu^{3+} ion in accordance with the variation of the radius of the lanthanide ions. Six cyanide ligands surround the Cr^{3+} ion in a distorted octahedral environment. Each $[Cr(CN)_6]$ unit coordinates to two Ln^{3+} ions using two trans cyanide ligands, while each $Ln(H_2O)_4$(bpy) group connects two $[Cr(CN)_6]$ moieties in a cis fashion, yielding a chain. A schematic view of the chain of $[NdCr]_n$ is shown as an example in Figure 2b. The angles Ln−Cr−Ln and the Cr−Ln−Cr have the same value in each compound (159.55° for **4′**, 159.41° for **5**, 159.30° for **6**, 159.20° for **7**, 159.14° for **8**, 159.02° for **9**, 158.99° for **10**, 158.96° for **11**, 158.93° for **12**, and 158.88° for **13**). Each lanthanide ion has two different intramolecular distances with each of the two neighboring chromium(III) ions, and, thus, the chain could be considered as an alternating one (5.656 and 5.759 Å for **4′**, 5.644 and 5.744

Table 5. Selected Bonds Lengths (Å) and Angles (deg) for **4′**−**13**

	4′	5	6	7	8	9	10	11	12	13
Ln−O(1)	2.451(3)	2.426(2)	2.414(4)	2.386(4)	2.372(2)	2.360(2)	2.353(3)	2.330(3)	2.342(2)	2.334(3)
Ln−O(2)	2.476(3)	2.447(2)	2.442(3)	2.409(4)	2.390(2)	2.379(2)	2.372(3)	2.355(3)	2.345(2)	2.341(3)
Ln−O(3)	2.449(3)	2.418(2)	2.408(4)	2.392(4)	2.369(2)	2.363(2)	2.361(2)	2.345(3)	2.344(2)	2.337(3)
Ln−O(4)	2.415(3)	2.385(2)	2.380(4)	2.345(4)	2.326(2)	2.313(2)	2.302(3)	2.289(3)	2.284(2)	2.273(3)
Ln−N(1)	2.625(4)	2.602(2)	2.593(4)	2.562(5)	2.549(2)	2.527(2)	2.533(3)	2.519(3)	2.514(3)	2.503(4)
Ln−N(2)	2.605(4)	2.571(2)	2.566(4)	2.531(5)	2.521(2)	2.523(2)	2.507(3)	2.487(3)	2.481(3)	2.467(4)
Ln−N(3)	2.536(4)	2.520(2)	2.507(4)	2.466(6)	2.461(2)	2.436(3)	2.437(3)	2.426(3)	2.419(3)	2.411(4)
Ln−N(8)	2.542(4)	2.512(2)	2.493(5)	2.455(5)	2.445(2)	2.436(3)	2.416(3)	2.411(3)	2.404(3)	2.384(4)
Cr−C(11)	2.075(5)	2.086(2)	2.076(5)	2.077(7)	2.085(3)	2.083(3)	2.082(4)	2.081(4)	2.091(3)	2.085(5)
Cr−C(12)	2.082(5)	2.085(3)	2.084(5)	2.078(6)	2.083(2)	2.082(3)	2.082(3)	2.076(4)	2.087(4)	2.074(5)
Cr−C(13)	2.082(5)	2.080(3)	2.089(5)	2.077(6)	2.080(2)	2.072(3)	2.082(4)	2.079(4)	2.059(4)	2.084(5)
Cr−C(14)	2.061(5)	2.062(3)	2.056(5)	2.056(6)	2.058(2)	2.067(3)	2.075(4)	2.065(4)	2.076(4)	2.057(5)
Cr−C(15)	2.070(5)	2.076(3)	2.074(5)	2.066(6)	2.075(3)	2.070(3)	2.085(4)	2.074(4)	2.088(4)	2.076(5)
Cr−C(16)	2.064(5)	2.082(2)	2.066(5)	2.090(7)	2.075(3)	2.077(3)	2.089(4)	2.074(4)	2.086(3)	2.079(5)
N(3)−C(11)	1.161(7)	1.148(3)	1.148(7)	1.162(8)	1.146(3)	1.149(4)	1.154(5)	1.151(5)	1.150(4)	1.141(7)
C(11)−N(3)−Ln	174.5(4)	175.6(2)	175.2(4)	175.4(5)	175.6(2)	175.8(2)	175.9(3)	176.1(3)	176.0(3)	175.9(4)
N(3)−C(11)−Cr	175.3(4)	175.3(2)	175.6(4)	174.5(5)	175.0(2)	174.7(2)	174.8(3)	174.3(3)	174.8(3)	174.6(4)

Å for **5**, 5.621 and 5.720 Å for **6**, 5.598 and 5.692 Å for **7**, 5.585 and 5.680 Å for **8**, 5.578 and 5.657 Å for **9**, 5.565 and 5.660 Å for **10**, 5.553 and 5.646 Å for **11**, 5.552 and 5.649 Å for **12**, and 5.530 and 5.626 Å for **13**, respectively**)**. Between the chains, there are water and bpy crystallization molecules. Note that the bpy of crystallization adopts two different stereo configurations. One of them is not planar and shows a dihedral angle (N−C−C−N) of 20.5 for **4′**, 18.8° for **5**, 18.3° for **6**, 19.4° for **7**, 18.2° for **8**, 18.6° for **9**, 17.9° for **10**, 18.1° for **11**, 17.1° for **12**, and 16.5° for **13**.

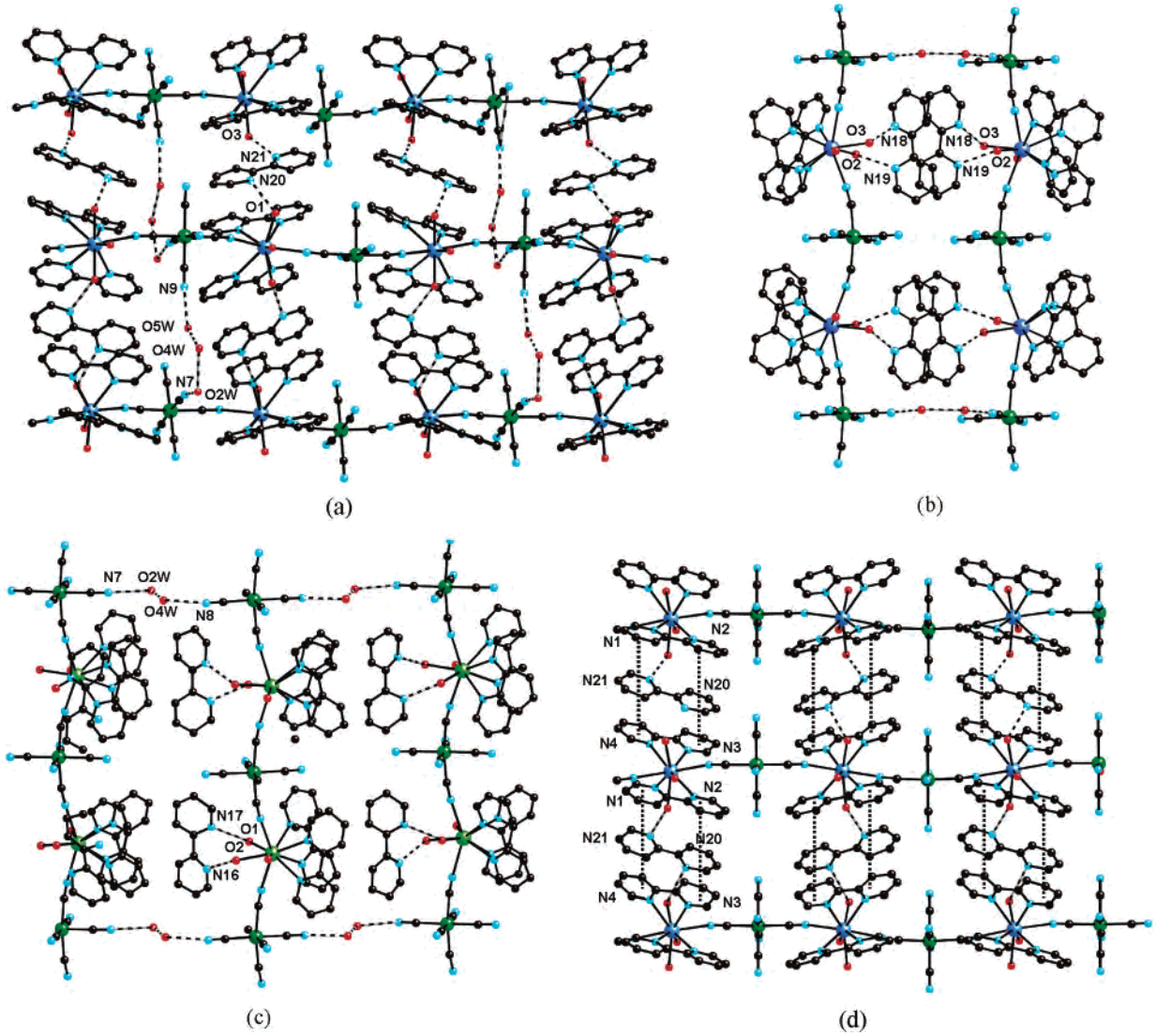

Figure 3. For complex **1**, schematic represention of some of the different pathways in which the chains are self-assembled through hydrogen bonds (a), (b), and (c) and one set of $\pi-\pi$ interactions (d). Complexes **2**−**4** show similar $\pi-\pi$ interactions.

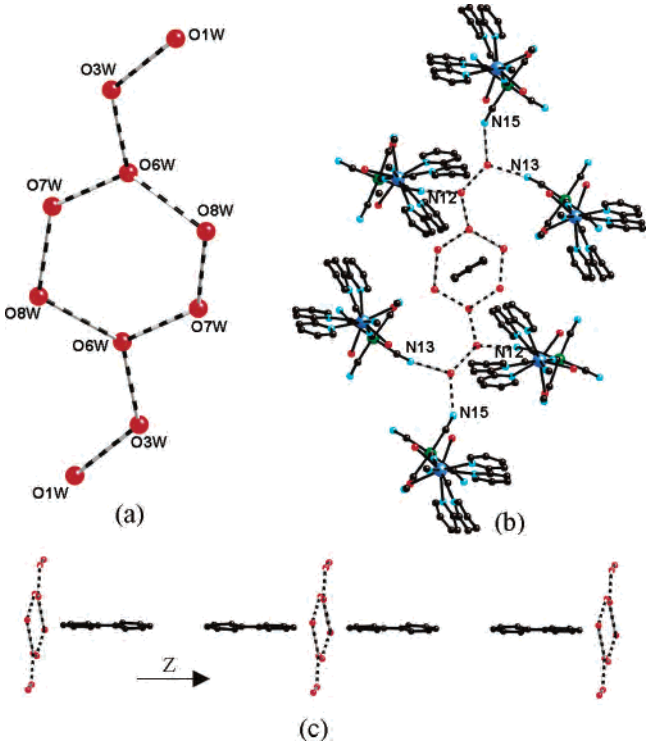

Figure 4. (a) Perspective view of water decamer showing the atom numbering scheme. (b) Perspective view down the *z* axis of the 3D hydrogen polymer formed between $(H_2O)_{10}$ and **1** chains. (c) A view showing the bpy ligands (N22−N23) and the decamer $(H_2O)_{10}$ occupying the cavities of the crystal in the *z* direction.

The other configuration is planar and the same dihedral angle is 180°. Bond lengths and angles of the bpy ligand are similar to those observed in the free bpy molecules when the abnormal trans configuration is taken into account. A supramolecular 3D network is given by the hydrogen bonds involving the nitrogen atoms of the bpy molecules of crystallization (N9, N10, N11), the four oxygen atoms (O1, O2, O3, O4) of the water ligands of the $Ln(H_2O)_4(bpy)$ entity, the nitrogen atoms (N4, N5) of two terminal CN^- ligands of the $[Cr(CN)_6]$ entity, and the O1S of water molecules of crystallization. An example of these 10 isomorphous complexes (Figure 5) shows the different ways as well as the atoms involved in the 3D self-assembled structure through hydrogen bonds for complex $[HoCr]_n$. Hydrogen bond distances are shown in Supporting Information (Table S2) for complexes **4′**−**13**. The *trans*-bpy of crystallization (N11) and the bpy ligands of two neighboring chains (N1, N2) exhibit a weak $\pi-\pi$ interaction (Supporting Information, Figure S1a). These interactions prove that the bpy ligands are situated along the chain in the cis position. A $\pi-\pi$ interaction between each of the neighboring nonplanar bpy of crystallization (N9, N10) also is present in the crystal. This interaction, together with the hydrogen bonds between O(2)−N(9) and O(3)−N(10), joins the chains by pairs (Supporting Information, Figure S1b). These $\pi-\pi$ interactions provide additional stabilization of the crystal structure. Intermolecular stacking distances between centroids of the bpy rings are shown for complexes **4′**−**13** in Table 6. Complexes **4′**−**13** are isostructural with the $[GdCr]_n$ previously reported.[8b]

Magnetic Studies. Magnetic measurements were performed for all the $[LnCr]_n$ complexes. With the exception of the Gd^{3+} ion, the paramagnetic lanthanide(III) ions possess a first-order orbital angular momentum that prevents the use of a spin-only Hamiltonian for isotropic exchange.

Not much is known about the nature of the exchange interaction of rare earth ions between themselves and with other magnetic groups, because the large orbital contribution of these ions makes a quantitative interpretation of the magnetic data of their complexes very complicated. Furthermore, because of the inner nature of the 4f orbitals with respect to the 3d ones, these ions usually are involved in weak exchange-coupling interactions. The magnitude of these interactions is comparable with that arising from the crystal field splitting of the ground *J* multiplet of the ion. The difficulty of gathering quantitative information on both these contributions thus far has reduced the analysis of the magnetic properties of the anisotropic lanthanides mainly to a qualitative level especially in molecular complexes. The most diffuse experimental approach to separate the different contributions of the crystal field and the exchange-coupling to the magnetic properties in either heterometallic or lanthanide-radical complexes involves the determination of magnetic properties of a corresponding complex in which the second spin carrier is substituted by a diamagnetic analogue that gives rise to comparable ligand field effects on the lanthanides.[5b,5c,8a,8c,25,26]

Previously, we reported the reaction of $K_3[Co(CN)_6]$, $Ln(NO_3)_3$, and bpy as the blocking ligand with the same reaction conditions as the complexes synthesized in the present paper.[6d,8a,8c] The early lanthanide ions of the series gave trinuclear complexes of the formula *trans*-$[Co(CN)_4(\mu\text{-}CN)_2\{Ln(H_2O)_4(bpy)_2\}_2][Co(CN)_6]\cdot 8H_2O$ (Ln = La^{3+}, Ce^{3+}, Pr^{3+}, Nd^{3+}, and Sm^{3+}). The remaining lanthanide ions gave 1D structures of the formula trans-$[Co(CN)_4(\mu\text{-}CN)_2Ln(H_2O)_4(bpy)]_n\cdot 4nH_2O\cdot 1.5n$bpy (Ln = Eu^{3+}, Tb^{3+}, Dy^{3+}, Ho^{3+}, Er^{3+}, Tm^{3+}, Gd^{3+}, and Yb^{3+}).

The approach consists of comparing their magnetic susceptibility data with the corresponding isostructural [LnCo] compounds together with the magnetic properties of the [LaCr] or [LuCr] complexes to take into account the magnetic behavior of the Cr^{3+} ion in the same crystalline field. It was impossible to apply the typical empirical approach that was mentioned above to the complexes **2**, **3**, **4**, and **5**. These complexes are not isostructural with the analogous compounds of cobalt(III) but are rather trinuclear in structure.

The comparison of the experimental magnetization of the exchange-coupled system at low temperature with that of the corresponding uncorrelated spin systems constitutes an additional way to discriminate the sign of the coupling. Specifically, the experimental magnetization of every $[LnCr]_n$ compound is compared with the sum of the $[LnCo]_n$ and $[LuCr]_n$ magnetization curves, that is, the uncorrelated spin

(25) *International Tables of X-ray Crystallography;* Ed. Kynoch Press, 1974, Vol. IV, pp 99−100 and 149.
(26) (a) Costes, J. P.; Dahan, F.; Dupuis, A.; Laurent, J. P. *Chem.—Eur. J.* **1998**, *9*, 1616. (b) Caneschi, A.; Dei, A.; Gatteschi, D.; Poussereau, S.; Sorace, L. *Dalton Trans.* **2004**, 1048 and references therein.

Table 6. Distances between bpy Ring Centroid (Å) for Complexes **1**−**4**,[a] **4′**−**13**[b]

	1	**2**	**3**	**4**
Cg(1)−Cg(10)	3.588	3.573	3.573	3.603
Cg(2)−Cg(9)	3.764	3.745	3.798	3.846
Cg(3)−Cg(9)	3.605	3.665	3.667	3.618
Cg(4)−Cg(10)	3.567	3.558	3.550	3.5607
Cg(7)−Cg(7)	3.521	3.486	3.532	3.4775
Cg(8)−Cg(8)	3.488	3.515	3.496	3.452

	4′	**5**	**6**	**7**	**8**	**9**	**10**	**11**	**12**	**13**
Cg(1)−Cg(5)	3.667	3.678	3.677	3.657	3.657	3.667	3.655	3.648	3.661	3.647
Cg(2)−Cg(5)	3.574	3.616	3.614	3.597	3.614	3.623	3.611	3.610	3.650	3.628
Cg(3)−Cg(4)	3.954	3.934	3.926	3.916	3.912	3.924	3.901	3.889	3.890	3.872

[a] Cg(1), ring of N(1); Cg(2), ring of N(2); Cg(3) ring of N(3); Cg(4) ring of N(4); Cg(7) ring of N18, Cg(8) ring of N19; Cg(9), ring of N(20); Cg(10) ring of N(21). [b] Cg(1), ring of N(1); Cg(2), ring of N(2); Cg(3) ring of N(9); Cg(4) ring of N(10); Cg(5) ring of N(11).

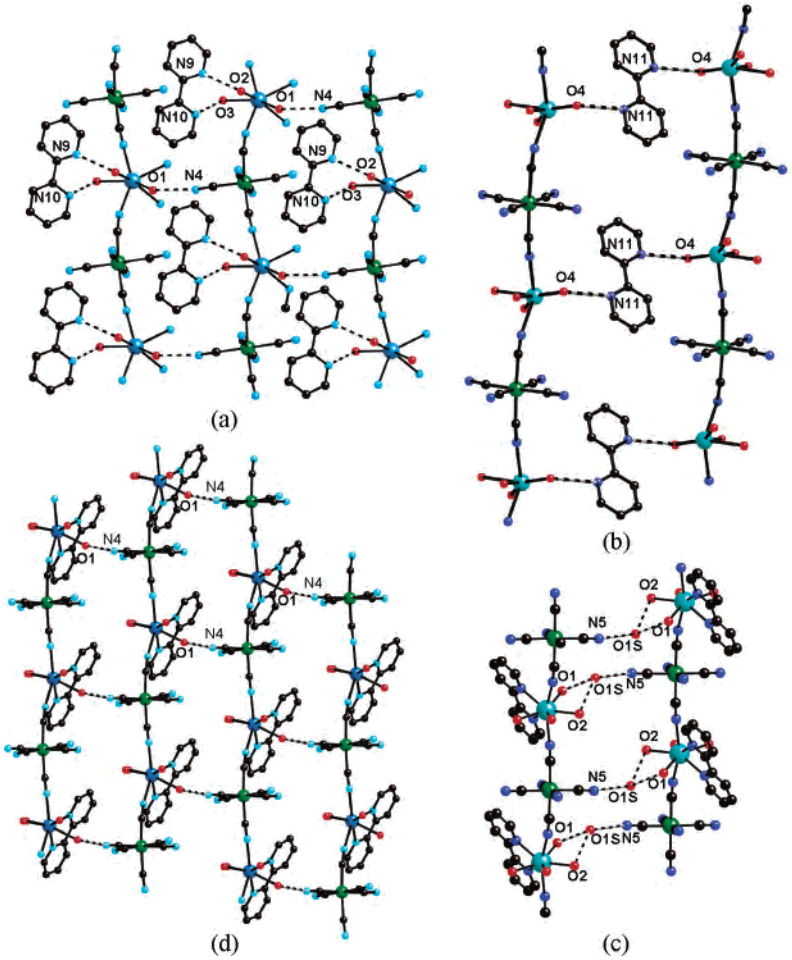

Figure 5. (a−d) For complex **9**, schematic representation of the different pathways in which the chains are self-assembled through hydrogen bonds.

systems. If the **M** vs **H** curve of the coupled system runs below the curve of the noncorrelated system, an antiferromagnetic interaction within the molecular spin system is revealed, while the reverse would be true for a ferromagnetic situation.[27]

Generally, in the lanthanide ions at room temperature, all Stark sublevels are thermally populated. As the temperature is lowered, a depopulation of these sublevels occurs and, consequently, $\chi_M T^{Ln}$ decreases. When the Ln^{3+} ion interacts with another paramagnetic species, the temperature dependence of $\chi_M T$ is because of both the variation of $\chi_M T^{Ln}$ and the coupling between the Ln^{3+} ion and the second spin carrier. Thus, it is difficult to conclude whether ferro- or antiferromagnetic interaction takes place when the approach described below cannot be applied.

For most of the rare earth compounds, the $\chi_M T$ value at room temperature is close to that predicted in the free-ion approximation for the cases in which only one level, $^{2S+1}L_j$, is thermally populated and second-order contributions are ignored.[28]

(27) Sutter, J. P.; Khan, M. L.; Khan, O. *Adv. Mater*. **1999**, *11*, 863.

(28) Kahn, O. *Molecular Magnetism*; VCH: Weinheim, Germany, 1993.

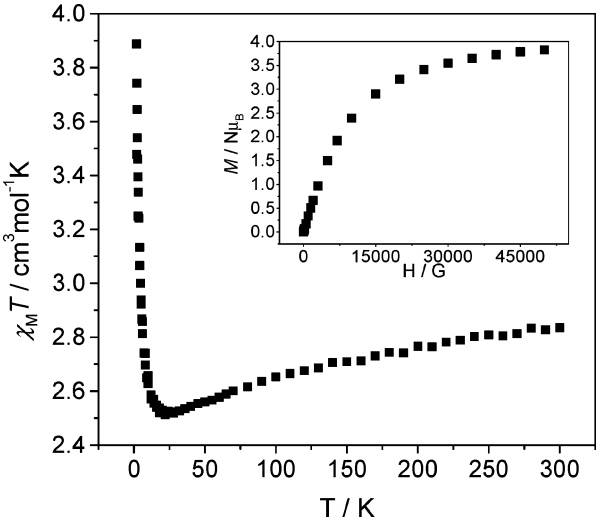

Figure 6. Thermal dependence at 8000 G of $\chi_M T$ for $[CeCr]_n$ (**2**). Inset: magnetization vs **H** of **2** at 2 K.

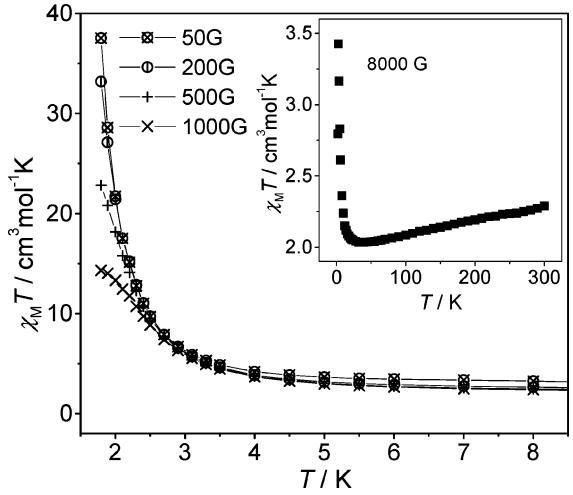

Figure 7. Thermal dependence at different fields (from 1000 to 50 G) of $\chi_M T$ for **5**

(a) Negligible Interaction. Complex 6. The Eu^{3+} ion has a nonmagnetic ground state, $^7F_0$, but there should be an important temperature-independent susceptibility because of close proximity of the low-lying excited states. A plot of $\chi_M T$ of the compounds $[EuCr]_n$ and $[EuCo]_n$ is shown in Supporting Information (Figure 2, top) together with $\chi_M T$ of $[LuCr]_n$ and $\Delta\chi_M T = \chi_M{}^{[EuCr]_n}T - \chi_M{}^{[EuCo]_n}T$. At 300 K, the $\chi_M T$ value of $[EuCr]_n$ is about 3.34 cm^3 mol^{-1} K, which is close to the expected value, for one isolated Eu^{3+} ion (the experimental value is in the range 1.44−1.62 cm^3 mol^{-1} K) and one isolated Cr^{3+} ion (the experimental value of the isostructural $[LuCr]_n$ complex is 1.98 cm^3 mol^{-1} K) and decreases with the temperature to 1.76 cm^3 mol^{-1} K at 2 K. The $\Delta\chi_M T$ and the $\chi_M{}^{[LuCr]_n}T$ curves are quasi-parallel, which indicates that there is negligible interaction between the spin carriers. Furthermore, the experimental magnetization of $[EuCr]_n$ (Supporting Information, Figure 2, bottom) is practically superimposable to that of the uncorrelated spin system.

Complex 12. A plot of the $\chi_M T$ of $[YbCr]_n$, $[YbCo]_n$, and $[LuCr]_n$ is shown Supporting Information (Figure S3), together with $\Delta\chi_M T$. At 300 K, the $\chi_M T$ value of the $[YbCr]_n$ is about 4.46 cm^3 mol^{-1} K, which is close to the expected value, in the free-ion approximation for one isolated Yb^{3+} ion (the calculated value is 2.57 cm^3 mol^{-1} K with a g value of 8/7) and one isolated Cr^{3+} ion and it decreases with the temperature to 3.27 cm^3 mol^{-1} K. $\Delta\chi_M T$ is practically superimposable with $\chi_M{}^{[LuCr]_n}T$, which indicates that there is negligible interaction between the spin carriers. Furthermore, the experimental magnetization of $[YbCr]_n$ (Supporting Information, Figure S3) is practically superimposable to that of the uncorrelated spin system.

(b) Antiferromagnetic interaction. Complex 2. The temperature dependence of $\chi_M T$ for **2** is shown in Figure 6. At 300 K, the $\chi_M T$ value is approximately equal to 2.84 cm^3 mol^{-1} K, which is close to the expected value, in the free-ion approximation for one isolated Ce^{3+} ion (the calculated value is 0.80 cm^3 mol^{-1} K with a g value of 6/7) and one isolated Cr^{3+} ion. When the temperature is lowered, it reaches a minimum of 2.52 cm^3 mol^{-1} K at approximately 29 K and then increases drastically to 3.83 cm^3 mol^{-1} K at 2 K. This behavior could be analogous to that observed in the ferrimagnets, but low-temperature magnetic measurements (zero field cooling−field cooling (ZFC−FC) and susceptibility measurements at a range of low magnetic fields) did not indicate the presence of ordering. The experimental magnetization of **2** at 2 K achieves a value of 3.83 Nμ_B at 5 T (Figure 6, inset). The magnetic behavior reflects an antiferromagnetic interaction between Cr^{3+} and Ce^{3+} ions to give a ferrimagnetic chain.

Complex 4. The temperature dependence of $\chi_M T$ for **4** is shown in Supporting Information (Figure S4). At 300 K, the $\chi_M T$ value is approximately equal to 3.90 cm^3 mol^{-1} K, which is close to the expected value, in the free-ion approximation for one isolated Nd^{3+} ion (the calculated value is 1.64 cm^3 mol^{-1} K with a g value of 8/11) and one isolated Cr^{3+} ion. When the temperature is lowered, it reaches a minimum of 2.98 cm^3 mol^{-1} K at approximately 20 K and then increases drastically to 4.71 cm^3 mol^{-1} K at 2 K. This behavior could be analogous to that observed in the ferrimagnets, but low-temperature magnetic measurements (ZFC−FC) and susceptibility measurements at a range of low magnetic fields) did not indicate the presence of ordering. The experimental magnetization of **4** at 2 K achieves a value of 4.40 Nμ_B at 5 T (Supporting Information, Figure S4, inset). The magnetic behavior reflects a ferrimagnetic character of the [Nd^{3+}−Cr^{3+}] interaction.

Complex 5. The temperature dependence of $\chi_M T$ for **5** at 8000 Oe is shown in Figure 7 (inset). The $\chi_M T$ value at 300 K is about 2.29 cm^3 mol^{-1} K. This value is inconsistent with the theoretical value of 0.09 cm^3 mol^{-1} K expected for one independent Sm^{3+} ($^7F_0$) ion. The disagreement is ascribed to the presence of thermally populated excited states, which is well-known for Sm^{3+} complexes. When the temperature is lowered, the $\chi_M T$ value reaches a minimum of 2.04 cm^3 mol^{-1} K at approximately 36 K and then increases drastically to 3.42 cm^3 mol^{-1} K at 2 K. Susceptibility measurements at low temperatures were carried out at a range of low magnetic fields (Figure 7). When the magnetic field decreased from

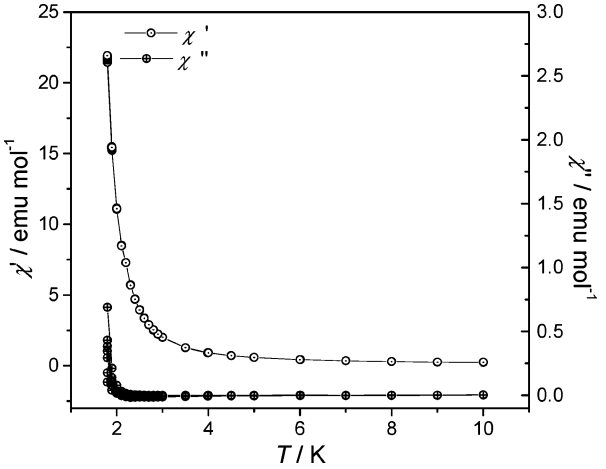

Figure 8. Plot of the in-phase (χ') and out-of-phase (χ'') components of the ac susceptibility of **5**, at 1500, 1250, 1000, 750, 500, 100, and 50 Hz.

1000 to 50 Oe, the $\chi_M T$ value increased from 14.32 to 37.53 $cm^3\ mol^{-1}\ K$ at 2 K, which indicates the onset of a weak ferromagnetic 3D ordering possibly due to interchain interactions mediated by hydrogen bonds and/or $\pi-\pi$ stacking. In the alternating current (ac) measurements, a signals of χ'' appears that does not show any dependence on the frequency (Figure 8). A maximum in the χ'' vs T curve it is not observed, so we could conclude that the magnetic transition temperature, T_c, is lower than 2 K. The magnetic measurements are reproducible with different samples coming from different preparations and when the powder is pressed into a pellet to prevent preferential crystalline orientation with the magnetic field.

Complex 7. For the case of the **7**, the temperature dependence of $\chi_M{}^{[TbCr]_n}T$, $\chi_M{}^{[TbCo]_n}T$, and $\Delta\chi_M T$ are shown in Figure 9 (top). At 300 K, the $\chi_M T$ value of **7** is about 13.75 $cm^3\ mol^{-1}\ K$, which is close to the expected value, in the free-ion approximation for one isolated Tb^{3+} ion (the calculated value is 11.82 $cm^3\ mol^{-1}\ K$ with a g value of 3/2) and one isolated Cr^{3+} ion, and it decreases with the temperature to 3.14 $cm^3\ mol^{-1}\ K$. From approximately 150 K, $\Delta\chi_M T$ decreases with regard to the $\chi_M{}^{[LuCr]_n}T$. This profile of the $\Delta\chi_M T$ curve clearly shows that a weak antiferromagnetic interaction takes place. Furthermore, the experimental magnetization of **7** at 2 K (Figure 9, bottom) is lower than that of the uncorrelated spin system corroborating the antiferromagnetic coupling.

Complex 8. For the case of **8**, the temperature dependence of $\chi_M{}^{[DyCr]_n}T$, $\chi_M{}^{[DyCo]_n}T$, and $\Delta\chi_M T$ are shown in Supporting Information (Figure S5). At 300 K, the $\chi_M T$ value of **8** is about 16.48 $cm^3\ mol^{-1}\ K$, which is close to the expected value, in the free-ion approximation for one isolated Dy^{3+} ion (the calculated value is 14.17 $cm^3\ mol^{-1}\ K$ with a g value of 4/3) and one isolated Cr^{3+} ion; it decreases with the temperature to 5.11 $cm^3\ mol^{-1}\ K$. From approximately 100 K, $\Delta\chi_M T$ decreases with regard to the $\chi_M{}^{[LuCr]_n}T$. This profile of the $\Delta\chi_M T$ curve clearly shows that a weak antiferromagnetic interaction takes place. Furthermore, the experimental magnetization of **8** at 2 K (Supporting Information, Figure S5, bottom) is lower than that of the uncorrelated spin system corroborating the antiferromagnetic coupling.

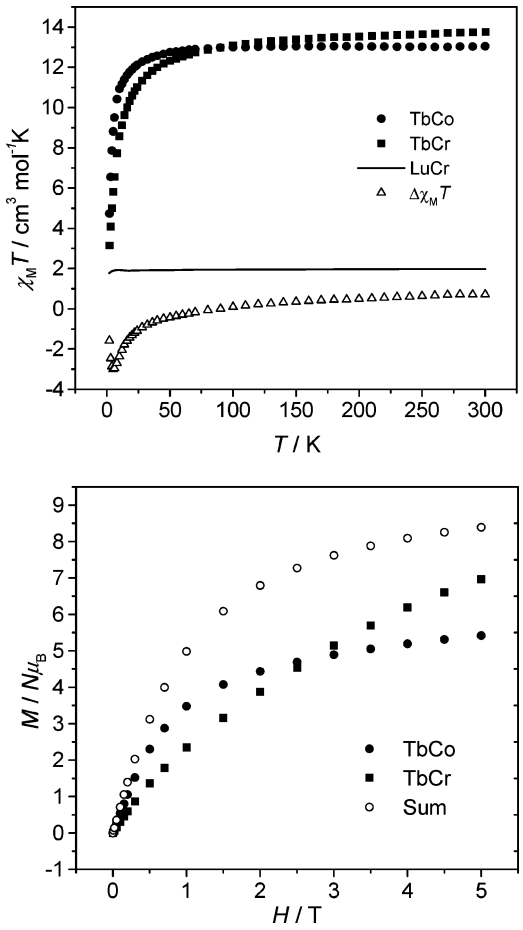

Figure 9. Top: thermal dependence at 800 G of $\chi_M T$ of **7**, $[TbCo]_n$, **13**, and $\Delta\chi_M T = \chi_M T^{[TbCr]_n} - \chi_M T^{[TbCo]_n}$. Bottom: magnetization vs **H** of $M^{[TbCr]_n}$, $M^{[TbCo]_n}$, and sum $= M^{[EuCo]_n} + M^{[LuCr]_n}$.

Complex 9. A plot of the $\chi_M T$ of $[HoCr]_n$, $[HoCo]_n$, and $[LuCr]_n$ is shown in Supporting Information (Figure S6, top) together with $\Delta\chi_M T$. At 300 K, the $\chi_M T$ value of **9** is about 15.90 $cm^3\ mol^{-1}\ K$, close to the expected value, in the free-ion approximation for one isolated Ho^{3+} ion (the calculated value is 14.07 $cm^3\ mol^{-1}\ K$ with a g value of 5/4) and one isolated Cr^{3+} ion; it decreases with temperature to 2.94 $cm^3\ mol^{-1}\ K$. From approximately 100 K, $\Delta\chi_M T$ decreases with regard to the $\chi_M{}^{[LuCr]_n}T$. This profile of the $\Delta\chi_M T$ curve clearly shows that a weak antiferromagnetic interaction takes place. Furthermore, the experimental magnetization of **9** at 2 K (Supporting Information, Figure S6, bottom) is lower than that of the uncorrelated spin system corroborating the antiferromagnetic coupling.

Complex 10. A plot of the $\chi_M T$ of $[ErCr]_n$, $[ErCo]_n$, and $[LuCr]_n$ is shown in Supporting Information (Figure S7, top) together with $\Delta\chi_M T$. At 300 K, the $\chi_M T$ value of **10** is about 13.45 $cm^3\ mol^{-1}\ K$, which is closed to the expected value, in the free-ion approximation for one isolated Er^{3+} ion (the calculated value is 11.48 $cm^3\ mol^{-1}\ K$ with a g value of 6/5) and one isolated Cr^{3+} ion; it decreases with the temperature to 7.52 $cm^3\ mol^{-1}\ K$. From approximately 75 K, $\Delta\chi_M T$ decreases with regard to the $\chi_M{}^{[LuCr]_n}T$. This profile of the $\Delta\chi_M T$ curve shows that very small antiferromagnetic interaction takes place. Furthermore, the experimental magnetization of $[ErCr]_n$ at 2 K (Supporting Information, Figure

Table 7. Nature of the Magnetic Interaction Between Ln^{3+} and Cr^{3+} and Comparison with Other Pairs

LnFe	Ce	Pr	Nd	Sm	Eu	Gd	Tb	Dy	Ho	Er	Tm	Yb
[LnFe][a]	AF	NI	AF	NI	NI	AF	F	AF	F	NI	F	NI
$[LnFe]_n$[b,c]	NI[b]	NI[b]	NI[b]	AF*[c]	NI[d]	AF[c]	AF[d]	AF*[d]	NI[d]	NI[d]	NI[d]	?[c]
$[LnCr]_n$[d,e]	AF[f]	?[f]	AF[f]	AF*[f]	NI[f]	AF[e]	AF[f]	AF[f]	AF[f]	AF[f]	AF[f]	NI[f]

* = ferrimagnet. F = ferromagnetic interaction. AF = antiferromagnetic interaction. NI = negligible interaction. ? = unresolved interaction. [a] Ref 5b. [b] Ref 6d. [c] Ref 8a. [d] Ref 8c. [e] $J = -0.52$ cm^{-1} ref 8b. [f] This work.

S7, bottom) is lower than that of the uncorrelated spin system corroborating the small antiferromagnetic coupling.

Complex 11. A plot of the $\chi_M T$ of $[TmCr]_n$, $[TmCo]_n$, and $[LuCr]_n$ is shown in Supporting Information (Figure S8, top) together with $\Delta\chi_M T$. At 300 K, the $\chi_M T$ value of **11** is about 9.19 cm^3 mol^{-1} K, which is close to the expected value, in the free-ion approximation for one isolated Tm^{3+} ion (the calculated value is 7.15 cm^3 mol^{-1} K with a g value of 7/6) and one isolated Cr^{3+} ion; it decreases with the temperature to 4.68 cm^3 mol^{-1} K. The $\chi_M{}^{[LuCr]_n}T$ is almost superimposable to the $\Delta\chi_M T$ to 24 K after which the temperature $\Delta\chi_M T$ decreases to the value of 0.82 cm^3 mol^{-1} K. This feature may be because of antiferromagnetic interchain interactions due to hydrogen bonds. The experimental magnetization of **11** (Supporting Information, Figure S8, bottom) is lower than that of the uncorrelated spin system. Therefore, in this case, we propose that the antiferromagnetic intrachain interaction is the dominant interaction at low temperatures.

(c) Unresolved interaction. Complex 3. The temperature dependence of $\chi_M T$ of **3** is shown (Supporting Information, Figure S9). At 300 K, the $\chi_M T$ value is approximately equal to 3.65 cm^3 mol^{-1} K, which is close to the expected value, in the free-ion approximation for one isolated Pr^{3+} ion (the calculated value is 1.60 cm^3 mol^{-1} K with a g value of 4/5) and one isolated Cr^{3+} ion; it decreases with the temperature to 2.23 cm^3 mol^{-1} K at 2 K. The experimental magnetization of **3** at 2 K achieves a value of 3.45 $N\mu_B$ at 5 T (Supporting Information, Figure S9, inset). The shape of these curves, together with the lack of its isostructural Co(III) complex, dismisses any possibility of a sign of magnetic coupling.

Conclusions

Fourteen $[CrLn]_n$ 1D systems have been characterized and magnetically studied. The early lanthanide(III) ions (La−Nd) of the series gave 1D systems in which the coordination number was nine (three oxygen atoms from the three water molecules, four nitrogen atoms from the two bpy molecules, and two nitrogen atoms from the two cyanide-bridged ligands). The remaining lanthanide(III) ions (Sm−Lu as well as Nd) gave 1D structures in which the coordination number was eight (four oxygen atoms from the four water molecules, two nitrogen atoms from a bpy molecule, and two nitrogen atoms from the two cyanide-bridged ligands). After the two geometries were compared, the eight coordination was achieved by losing a bpy molecule and by adding a water molecule. Throughout the lanthanide series, a contraction of the radium values was manifested, so a diminution in the coordination number may be justified. In the works previously published by us, the complexes using $[Fe(CN)_6]^{3-}$ and $[Co(CN)_6]^{3-}$ with dimethylformamide (DMF) as a blocking ligand (monodentate), were found to have no changes in the full lanthanide series, but when the blocking ligand was bpy (bidentate), the early lanthanide ions gave trinuclear structures with coordination number of nine. The rest of the lanthanide ions have 1D structures with the coordination number of eight, so the bpy ligand played an important role in building the structure. For complexes **1**−**4**, we have characterized a discrete decameric water cluster that was built around a cyclic hexameric core, which represented another new mode of association of water molecules. The water cluster gained stability from strong hydrogen-bonding interactions with the available nitrogen atoms of the terminal cyanide ligands of neighboring chains. Thus, it appeared that the water cluster acted as a template around pack of chains and vice versa.

Most of the 3d−4f complexes that have shown long-range magnetic ordering involved the Sm^{3+} ion. In the systems of this work, very weak long-range magnetic ordering was observed in **5**. Table 7 summarizes the magnetic results obtained on the full lanthanide series using $[Fe(CN)_6]^{3-}$ and DMF[5b] or bpy as the blocking ligand[6d,8a,8c] and includes new findings concerning the Ln−Cr 1D systems together with the isostructural complex $[Gd-Cr]_n$, which was previously reported.[8b]

Acknowledgment. This work was financially supported by the Spanish Governement (Grant BQU2003-00539). We also thank Núria Clos, Sevei de Magnetoquímica, Serveis Científics i Tècnics, Universitat de Barcelona, for the magnetic measurements.

Supporting Information Available: Additional tables and Figures. This material is available free of charge via Internet at http://pubs.acs.org.

IC060942Q